ACS APPLIED MATERIALS & INTERFACES

Research Article

www.acsami.org

Energy Storage Studies on $InVO_4$ as High Performance Anode Material for Li-Ion Batteries

M. V. Reddy,*[,†,§,⊥] Bryan Lee Wei Wen,[†,‡] Kian Ping Loh,[§] and B. V. R. Chowdari[†]

[†]Department of Physics, Solid State Ionics/Advanced Batteries Lab, [§]Department of Chemistry, Graphene Research Center, and [⊥]Department of Materials Science & Engineering, National University of Singapore, Singapore 117542

[‡]River Valley High School, 6 Boon Lay Avenue, Singapore 649961

Supporting Information

ABSTRACT: $InVO_4$ has attracted much attention as an anode material due to its high theoretical capacity. However, the effect of preparation methods and conditions on morphology and energy storage characteristic has not been extensively investigated and will be explored in this project. $InVO_4$ anode material was prepared using five different preparation methods: solid state, urea combustion, precipitation, ball-milling, and polymer precursor methods. Morphology and physical properties of $InVO_4$ were then analyzed using X-ray diffraction (XRD), scanning electron microscope (SEM), and Brunauer–Emmett–Teller (BET) surface area method. XRD patterns showed that orthorhombic phased $InVO_4$ was synthesized. Small amounts of impurities were observed in methods II, III, and V using XRD patterns. BET surface area ranged from 0.49 to 9.28 $m^2\ g^{-1}$. SEM images showed slight differences in the $InVO_4$ nanosized crystalline structures with respect to preparation methods and conditions. Energy storage studies showed that, among all the preparation methods, the urea combustion method produced the best electrochemical results, with negligible capacity fading between the 2nd and 50th cycles and high capacity of 1241 mA h g^{-1} at the end of the 20th cycle, close to the theoretical capacity value. Precipitation method also showed good performance, with capacity fading (14%) and capacity of 1002 mA h g^{-1} at the 20th cycle. Cyclic voltammetry (CV) and electrochemical impedance spectroscopy (EIS) was then used to determine the reaction mechanisms of $InVO_4$.

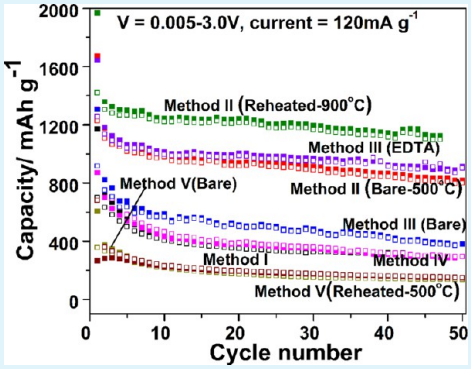

KEYWORDS: *$InVO_4$, lithium-ion batteries, anodes, energy storage, preparation methods, electro-analytical techniques*

INTRODUCTION

Lithium-ion batteries are considered to be one of the most important energy storage and conversion technologies today, with a high energy density and long cycling life, as well as being rechargeable.[1,2] As a result, Li-ion batteries have enjoyed huge commercial success and are the present-day choice in a wide range of portable electronic appliances and consumer products, including laptops, phones, electric hybrid vehicles, and for the military. Commercial Li-ion batteries use lithium cobalt oxide ($LiCoO_2$) as the cathode and graphite as the anode.[2,3] However, graphite has a relatively low theoretical capacity of 372 mA h g^{-1} and suffers from Li-dendrite formation during high current rates of cycling. Hence, there is a potential for graphite to be replaced with another anode material that will possibly enhance the performance of Li-ion batteries.

Researchers are currently finding different approaches to do so, like the use of metal oxides which undergoes alloying-dealloying and conversion reaction[2] to improve capacity values of such batteries. Indium Vanadate ($InVO_4$) has attracted much attention[4] as a potential substitute as anode material for Li-batteries since it undergoes conversion of indium, vanadium oxide, and alloying reactions of indium. As early as 1997, the Tarascon group reported the synthesis and electrochemical properties of vanadates, of which they highlighted $InVO_4$, with a high theoretical capacity of as large as 900 mA h g^{-1} (approximately 2.5 times greater than those obtained with conventional graphite electrodes) thus being a potential anode material for rechargeable Li-ion batteries.[4] Preliminary Li-cycling of $InVO_4$ was prepared using a chemical douce (coprecipitation) method, reported in ref 4. There have also been studies looking at creating novel chrysanthemumlike orthorhombic phase $InVO_4$ microstructures using the hydrothermal method.[5] However, there has not been much literature on a comparison between different preparation methods and how it would affect the physical and electrochemical properties and morphology of $InVO_4$.

In this project, the effect of preparation methods on morphology and electrochemical properties of $InVO_4$ will be analyzed. Characterization was done using X-ray diffraction (XRD), the Brunauer–Emmett–Teller (BET) surface area method, density measurements, and scanning electron

Received: April 24, 2013
Accepted: July 19, 2013
Published: July 19, 2013

   dx.doi.org/10.1021/am401501a | ACS Appl. Mater. Interfaces 2013, 5, 7777–7785

microscope (SEM) imaging, while electrochemical properties were studied using cyclic voltammetry and galvanostatic cycling. The method that synthesized the compound with the best properties to function as anode material was then further evaluated using impedance spectroscopy to understand more about the reaction kinetics and mechanism. Reaction mechanisms of the compound during charge and discharge are also then proposed. For the first time, the detailed studies on the effect of preparation methods and conditions on electrochemical properties of $InVO_4$ are reported.

EXPERIMENTAL SECTION

Preparation of $InVO_4$ Compounds. $InVO_4$ was prepared by different preparation methods to find out whether and how preparation conditions would affect the capacity and cycling stability. Reagent-grade compounds were used as supplied by different chemical suppliers with a purity of 98−99% for all of the following described methods. For easier identification during result analysis, the preparation methods will be named I, II, III, IV, and V as stated below, with the different preparation conditions in each method listed in brackets.

Preparation Using the Solid State Method (Method I). Stoichiometric amounts of indium(III) oxide (In_2O_3) and ammonium metavanadate (NH_4VO_3) in the mole ratio of 1:2 were mixed to obtain 4 g of active material. The final weighed mass was as follows: In_2O_3, 2.171 g; NH_4VO_3, 1.829 g. The compounds were pressed together into a pellet and heated in a platinum crucible at 1000 °C in air for 10 h and cooled for 12 h at room temperature. The pellets were then ground to powder using mortar and pestle.

Preparation Using the Urea Combustion Method (Method II). Stoichiometric amounts of In_2O_3, NH_4VO_3, and urea in mole ratio of 1:2:10 was calculated to obtain a total 6 g of active material. The final mass of each compound was as follows: In_2O_3, 2.637 g; NH_4VO_3, 2.222 g; urea, 11.41 g. In_2O_3 was dissolved in a minimum amount nitric acid (HNO_3) to convert In_2O_3 into $InNO_3$ before being mixed with ammonium vanadate (NH_4VO_3). The solution was then evaporated to dryness on a heating plate. The powder was heated at 500 °C and further reheated to 900 °C in air for 6 h and cooled at room temperature for 12 h. Both samples were used in the experimentation to look at the effect of reheating. The two samples will be named method II (bare-500 °C) and method II (reheated-900 °C) for the respective temperatures the samples were subjected to during preparation in this report.

Preparation Using the Precipitation Method (Method III). In_2O_3 was dissolved in a minimum amount of hydrochloric acid (HCl) and aqueous ammonia (NH_4OH) was added to get a white precipitate of In-hydroxide. It was recovered by filtration, dried, and mixed with vanadyl acetyl acetonate ($VO(acac)_2$), which is used as a reagent in the epoxidation of In-hydroxide. Ethalene diamine tetra aceto acetic acid (EDTA), used as a complexing agent, was added to half of the filtered dry sample. Both the products were heated at 500 °C for 6 h in air and cooled at room temperature. The two samples will be named method III (bare) and method III (EDTA) for the samples without and with the addition of EDTA, respectively.

Preparation Using the Ball-Milling Method (Method IV). Stoichiometric amounts of In_2O_3 and vanadium pentoxide (V_2O_5) in the ratio of 1:1 were calculated to obtain 3 g of total active material. The final mass was as follows: In_2O_3, 1.813 g, V_2O_5, 1.187 g. It was then ball-milled for 18 h with the weight ratio of 3 g powder:10 g balls, using a Spex Ballmiller (USA).

Preparation Using the Polymer Precursor Method (Method V). Stoichiometric amounts of In_2O_3, 2 M polyvinylpyrrolidone (PVP) and NH_4VO_3 were weighed and made up to form 6 g of active material. PVP was used as a dispersing and capping agent[6] as the polymer is easily soluble in water and the metal ion gets nicely dispersed in the presence of PVP.[7] The final mass of each compound was as follows: In_2O_3, 2.270 g; NH_4VO_3, 1.913 g; PVP, 1.817 g. These were dissolved in 60 mL ethylene glycol and 8 mL HNO_3 and dried on a hot plate at 200 °C, left for about 6 h. Half of this sample was then reheated in a tube furnace at 500 °C for 6 h. Both samples were used for experimentation and will be named method V (bare) and method V (reheated-500 °C).

Electrode Fabrication. The electrodes were fabricated using the synthesized $InVO_4$ as active material, polyvinylidene fluoride (PVDF) as a polymer binder (Kynar 2801), and Super-P carbon black (ENSACO, MMM Super P, 230 m^2 g^{-1}) with the weight ratio 70:15:15. The mixture was ground using a mortar and pestle to fine powder, and then dissolved in PVDF and organic solvent *N*-methyl-2-pyrrolidone (NMP, Alfa Aesar). *N*-methyl-2-pyrrolidinone was used as the solvent to disperse the $InVO_4$ powder, carbon black, and the binder It was then stirred with magnetic stirrer for 12 h resulting in uniform viscous slurry. The slurry was then coated onto an etched copper foil (Shenzhen Vanlead Tech. Co. Ltd., China) using the doctor blade technique and dried in the oven at 80 °C for 12 h. It was then roller-pressed using a twin roller machine. This was to increase contact between the electrode and copper foil. The coated copper foil was then cut into 16 mm diameter disks (2.0 cm^2) using an electrode cutter. Disks with the most uniform layer of composite material coated on them were chosen and weighed. The active material in each electrode was calculated by subtracting the mass of copper foil from it then multiplying the composition (70%).The electrodes were placed in a vacuum oven (OiLTEX) at 80 °C for 12 h before being fabricated into coin cells.

Coin Cell Fabrication. Coin cells (CR2016) were fabricated, using the electrode fabricated as the anode while 1 M lithium hexafluorophosphate ($LiPF_6$) dissolved in ethylene carbonate (EC) and dimethyl carbonate (DMC) in 1:1 volume ratio (Merck, Selectipur LP40) as electrolyte, lithium foil of 16.0 mm diameter and 0.595 mm thickness as the reference cathode, and Whatman filter paper (Aldrich) as a separator. The components were assembled using a coin cell crimper (Hosen, Japan) in the order of coin cell cap, anode, 10 μL electrolyte, separator, 10 μL electrolyte, lithium metal, spring, O-ring, and coin cell cover. This was done in an argon filled glovebox (MV150B-G, M-Braun). The coin cells were aged for 12 h before being cycled to electrochemical studies.[8−10]

Characterization Techniques. Structural properties of the $InVO_4$ synthesized from different preparation methods were characterized using XRD using a Philips X'PERT unit (PANalytical) with Cu K radiation (λ = 1.5405A) to investigate the lattice parameters and purity of the compound. The BET surface area method (Micrometrics TriStar 3000) was used to investigate the specific surface area and absorption properties of the material and density was recorded using a gas Pycknometer (Acupyc 1330, Micromerities, USA). SEM (JSM-67500F) was also used to investigate the surface morphology of the powder compounds. Electrochemical studies were carried out with 2016 type of coin cells using Bitrode battery tester using multichannel battery tester (Model MCV16-05/001-5, Bitrode, USA), and cyclic voltammetry (CV) studies were carried out using computer controlled terminals (Macpile II, Biologic, France) performed at the scan rate of 58 mV s^{-1} in the voltage window of 0.005−3.0 V at room temperature. Impedance spectroscopy was carried out with Solartron Impedance/gain-phase analyzer (model SI 1255) together with a potentiostat (SI 1268) at ambient room temperature of 25 °C. More details of the instrumentation are given in our previous reports.[11−14]

RESULTS AND DISCUSSION

Structure. The powder X-ray diffraction patterns of $InVO_4$ synthesized by different methods are shown in Figure 1, and color, different morphology and other physical properties as listed in Table 1. The prepared $InVO_4$ powders were brownish in color but became brighter (orange) colored upon reheating as seen in methods II and V. There is a clear trend observed BET surface area measurements, where reheating at a higher temperature consistently results in a decrease in BET surface area,

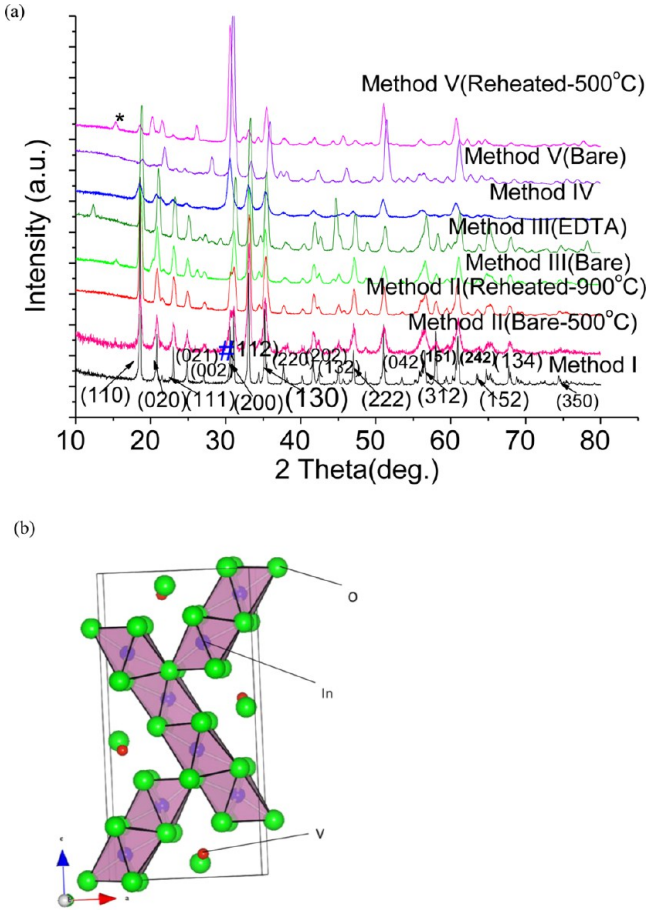

Figure 1. (a) XRD patterns of $InVO_4$ as prepared by different methods. Main (*hkl*) lines no. #(110) line of In_2O_3 and * (002) line of V_2O_5. (b) Crystallographic representation of $InVO_4$: red = vanadium, green = oxygen, and blue = indium.

as seen in methods II and V, from 9.27 to 0.49 $m^2\ g^{-1}$ and from 5.16 to 1.91 $m^2\ g^{-1}$, respectively. This might be because of the particles undergoing surface smoothening and densification upon annealing at higher temperatures due to grain growth. A similar decrease of BET surface area was noted with heat-treatment of a number of other metal oxides.[8,15] The experimental powder densities of all compounds are in the range 4.577−5.183 g cm^{-3}, while average crystallite sizes were relatively similar, from 13.7 to 32.2 nm. The small differences in the lattice parameter values, obtained by the Rietveld refinement of the powder XRD data, were due to the differences in the preparation methods (Table 1).

The Rietveld refinement of XRD data was done using the commercially available software TOPAS Version 2.1 (2000 Bruker AXS, Germany). The experimental XRD data of the different methods was refined using the orthorhombic $InVO_4$ structure with space group *Cmcm*(63) with parameters of $a \sim 5.76$, $b \sim 8.54$, and $c \sim 6.59$ Å to obtain the unit-cell lattice parameters as listed in Table 1. Experimental XRD patterns of $InVO_4$ were match with the refined data. Characteristic Bragg diffraction peaks distinctive of orthorhombic phase $InVO_4$ (JCPDF card 71-1689) could be seen for samples of $InVO_4$ in all methods used, as seen in Figure 1a. In addition to the original orthorhombic $InVO_4$ diffraction peaks, the refined XRD patterns of methods II, III, and V have peaks showing slight differences in the (*hkl*) peak intensity with respect to the preparation method. Further analysis using TOPAS software, the small impurity peaks observed were identified to be the In_2O_3 phase for all samples from methods I, II, and III and vanadium pentoxide (V_2O_5) for method V (reheated-500 °C). The formation of impurities such as In_2O_3 and V_2O_5 might arise due to the more acidic conditions of such methods since the pH in which preparation methods are carried out is critical to the phase purity of the synthesized compound[4] and other reaction conditions like preparation temperature, initial reactants etc. The general crystallographic representation of orthorhombic $InVO_4$ is shown in Figure 1b.

Morphology. SEM images of $InVO_4$ as prepared by different methods are shown in Figure 2a−h. The SEM images revealed that the $InVO_4$ particles were generally nanosized in the range of 100−300 nm in diameter, similar in particle size with previous studies on $InVO_4$ where hydrothermal reaction method was employed instead.[5] However, it is clearly seen that it varied in its particle nature and surface morphology with the different preparation methods employed.

Method I showed extensive coral-like structure morphology, which might be beneficial in faster diffusion pathway of Li-ion during conversion/alloying−dealloying reactions during charge and discharge cycles. Method II revealed agglomerated nanoparticles. These particles became more irregular after reheating at a higher temperature of 900 °C instead of 500 °C. Method III (with EDTA) also showed larger sized crystalline structures, which differs greatly from the same method without the addition of EDTA, as seen in Figure 2e, which were spherical-shaped individual particles and considerably smaller in particle size. This shows that EDTA acted as a good complexing agent, the use of which leads to differences in the crystallinity of the compound. Interestingly, method IV showed the presence of small papilla with estimated length of 500 nm emerging from the surface of the agglomerated particles. Nanobelts were also observed by Li et al.,[5] where hydrothermal reaction was used. Method V showed agglomerated particles with irregular cauliflowerlike shape. However, upon reheating at 500 °C for 6 h, the structure of compound in method V became more regular and cohesively layered. This was different from the morphology observed with the SEM images of method II, where reheating resulted in increase in irregularity of the particles instead. This might be due to the temperature of the preparation condition of the samples, since method II (bare) and method V (reheated-500 °C) were both prepared at 500 °C.

Energy Storage Studies. *Cyclic Voltammetry.* Cyclic Voltammetry is a technique that is recognized to study redox reaction couples and structural transformations during Li-intercalation/deintercalation of both cathode[16,17] as well as anode materials.[2,18,19] Cyclic voltammetry (CV) studies on $InVO_4$ were carried out at the scan rate of 58 mV s^{-1} in the voltage window of 0.005−3.0 V vs Li/Li^+ at room temperature to study electron transfer kinetics and transport properties. Li metal was used as the counter and reference electrode. The results of the cyclic voltammetry curves are shown in Figure 3a−h. For clarity, only selected cycles (1, 2, 3, and 6) are shown. All the samples showed very good reversible peaks. $InVO_4$ prepared using all the preparation methods produced a distinct and characteristic main anodic voltage peak at ∼0.68−0.71 V with different peak current intensities, as seen in Figure 3a−h is due dealloying of In. In addition, methods II and III also showed a second broad anodic peak at ∼1.20 V, which is not observable for the other methods I, IV, and V, while another anodic peak at 1.75−1.78 V was observed by methods II (reheated-900 °C)

Table 1. Structural and Physical Properties of $InVO_4$

sample	color of samples	BET surface area (±0.05 m^2/g)	average crystallite size (nm; by XRD)	density (g/cm^3)	lattice parameters (Å)
I	orange	9.23	23.1	5.0656	*a*: 5.723 (3)
					b: 8.512 (2)
					c: 6.499 (2)
II (bare-500 °C)	brown	9.275	19.5	4.6956	*a*: 5.734 (2)
					b: 8.590 (2)
					c: 6.527 (3)
II (reheated-900 °C)	brown	0.493	32.0	5.0334	*a*: 5.753 (2)
					b: 8.524 (3)
					c: 6.573 (2)
III (EDTA)	dark brown	0.579	32.2	4.5770	*a*: 5.760 (2)
					b: 8.534 (2)
					c: 6.523 (3)
III (bare)	dark brown	2.112	18.7	4.7944	*a*: 5.756 (3)
					b: 8.528(2)
					c: 6.567 (3)
IV	brown	3.156	13.7	5.0408	*a*: 5.736 (2)
					b: 8.546 (3)
					c: 6.512 (2)
V (bare)	brown	5.158	18.3	5.1832	*a*: 5.850 (3)
					b: 8.461 (2)
					c: 6.592 (3)
V (reheated-500 °C)	orange	1.913	16.6	5.2037	*a*: 5.756 (2)
					b: 8.528 (3)
					c: 6.567 (3)

and V. This might be due to other electrochemical reactions as will be proposed in the proposed reaction equations later. A single cathodic peak was observed at 0.25−0.68 V during the first cycles for all CV curves. These anodic and cathodic peaks shift to a higher voltage with an increase in cycle number from the second cycle onward. This indicates that after the amorphization[4] of $InVO_4$ in the first cycle, In and V particles are formed (eq 1) and In- and V-oxides are also formed during oxidation (eqs 3 and 4), which are then reduced at the second cycle onward (backward reactions of eq 3 and 4). A minor peaks is due to reduction of metal oxides to metals[2] and alloying/dealloying reactions[20] or reduction to lower oxidation states for ex VOx. A broad lines in the second and subsequent cycles are due to amorphous nature of material. We note further in situ complementatory spectroscopy techniques at various cathodic and anodic scan voltages of $InVO_4$ are needed to verify above observed reaction mechanism.

For method II, it can be observed that upon reheating at a higher temperature, the main anodic peak at 0.70 V became sharper and intensified, indicating better lithium ion conversion/alloying-dealloying reaction. The anodic peak of the first cycle for method III (bare) at 4.4 V was found to be broader as compared to method III (EDTA) due to the differences in the crystallinity of the samples. A double peak could be seen from the first cathodic scan of method V (reheated-500 °C) at 1.89 and 2.27 V as seen in Figure 3h. This might be due to the small amounts of V_2O_5 impurities (Figure 1). Previous studies have reported similar distinctive peaks for V_2O_5,[6,21] which further validates this conclusion. This demonstrated that the cathodic/anodic peak potentials are highly sensitive to morphology and crystal structure, and slight impurities would be observable in the cycling graphs.

Potentials obtained at which the alloying-dealloying reactions occur coincide with values determined from observing profile plateaus in galvanostatic cycling studies. CV of subsequent cycles shows a slight change in potential and a decreasing peak current intensity, which indicates the occurrence of capacity fading.

Galvanostatic Cycling Studies. In order to determine electrochemical properties of the different methods, galvanostatic cycling of the fabricated coin cells was done between 0.005 and 3.0 V vs Li/Li^+ with a current rate of 120 mA g^{-1}, which was carried out on coin cells, up to 60 cycles at room temperature. The open-circuit voltage (OCV) of the fabricated and aged cells is about 2.8−3.0 V. For clarity, only the comparative first and second cycles of all the different preparation methods and conditions are shown in Figure 4a and b, respectively, together with the capacity against cycle number graph as shown in Figure 5. The capacity values at the first and 20th cycles, and capacity fading is also given in Table 2. The full results of the galvanostatic cycling studies for the different preparation methods are provided in Supporting Information SI 1.

From the galvanostatic cycling results, an intercalation region is observed at ∼0.75 V in the first discharge cycle for all methods, as shown in Figure 4a. A plateau corresponding to the solid electrolyte interface (SEI) and alloying of In at low voltages of ∼0.20 V is also seen. It can be observed that method II also showed two small plateaus as compared to only one main plateau for the other methods. The method II sample as prepared at 900 °C had the two plateaus at ∼1.30 and ∼0.85 V vs Li, while the same method prepared at 500 °C gave a similar pattern but at a lower current of ∼1.20 and ∼0.75 V. Similar peaks was also observed for other metal oxides in previous studies.[2] This is due to the difference in the particle size and crystallinity upon reheating the sample, as seen in the SEM images previously (Figure.2).

Reversible capacity of the different methods varied from 606 to 1421 mAh g^{-1} at the first cycle, corresponding to 5.20 and 12.18 mol of Li respectively. Present observed capacity values

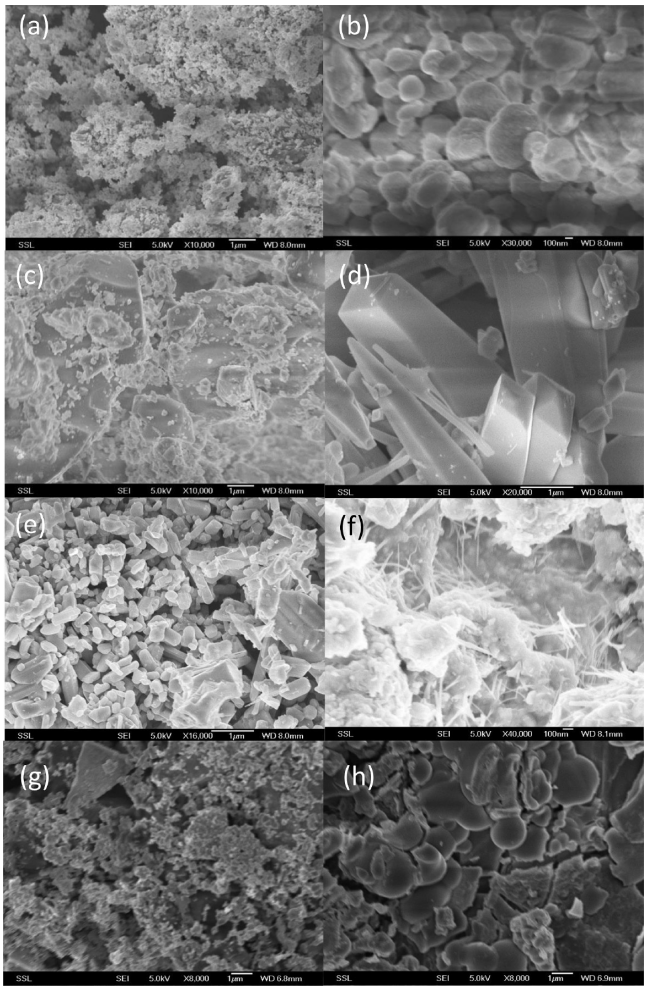

Figure 2. Selected SEM images of (a) method I, 13 000 magnification, bar scale 1 μm; (b) method II (bare-500 °C), 30 000 magnification, bar scale 100 nm; (c) method II (reheated-900 °C), 10 000 magnification, bar scale 1 μm; (d) method III (EDTA), 20 000 magnification, bar scale 1 μm; (e) method III (bare), 16 000 magnification, bar scale 1 μm; (f) method IV, 40 000 magnification, bar scale 100 nm; (g) method V (bare), 8 000 magnification, bar scale 1 μm; (h) method V (reheated-500 °C) 8 000 magnification, bar scale 1 μm.

are better than the previous reports,[5,4] which reported values of 608.6 and 900 mAh g^{-1} respectively for their first discharge capacity. Irreversible capacity-loss (ICL) during the initial first discharge−charge cycle was observed for all compounds. This can be attributed to (i) kinetic limitations of reactions 1−4[22,23] and (ii) the formation of SEI during the first discharge process, consuming extra Li-ions.[2,24] In addition, some of the coin cells evidently suffered from capacity fading in the first few cycles. This might be a result of the volume variations and crystal structure modifications during cycling, which is observed for many metal oxides undergoing conversion and alloying reactions,[2,25] resulting in a huge difference when comparing discharge capacity at first and the 20th cycle for some of the methods.

It was found that method II as prepared at 900 °C had the highest discharge capacity of 1241 mAh g^{-1} at the 20th cycle and also had the lowest capacity fading of 13% from second to the 50th cycle. The capacity value at 20th cycle is very close to the theoretical capacity of 1283 mAh g^{-1} (for 11 mol Li). In addition, method III with addition of EDTA and method II as prepared at 500 °C also showed comparable results of 1002 and 940 mAh g^{-1}, respectively, with a slightly higher capacity fading of 14.6% and 22%, respectively. $InVO_4$ compounds prepared by methods II and III have significantly smaller BET surface area as compared to those from the other preparation methods, implying that this smaller surface area might mean that it makes less side reactions with electrolyte. We note previous studies by Denis et al.[4] on $InVO_4$ sample with a surface area of 55 m^2/g showed higher irreversible capacity loss when compared to low surface area material (4 m^2/g) and they mentioned high surface area samples are prone to absorb moisture. In the present study in addition to surface area, preparation method and temperature is also play an important role on electrochemical properties. The other methods (I, IV, and V) experienced noticeable capacity fading, which resulted in a significant decrease in capacity values as compared to the first cycle. We note that in recent studies on molten salt synthesized $CuO{\cdot}Co_3O_4$ composites showed improved capacity when compared to bare $CuCo_2O_4$.[26] Further careful electrochemical studies on parent compounds, V_2O_5 and In_2O_3, under identical preparation method are needed to explain role of minor phases on energy storage properties of $InVO_4$. In general some of the following factors will play an important role on the electrochemical properties of $InVO_4$ are preparation method, initial reactants, morphology, crystal structure, and electrode fabrication method.

A reaction mechanism is proposed based on the charge/discharge reaction as well as CV studies.

$$InVO_4 + 8Li + 8e^- \rightleftharpoons In + V\,(\text{or VxOy}) + 4Li_2O \quad (1)$$

$$In + 3Li^+ + 3e^- \rightleftharpoons Li_3In \quad (2)$$

$$In + xLi_2O \rightleftharpoons In_2O_3 + xLi^+ + xe^- \quad (3)$$

$$V + Li_2O \rightleftharpoons V_2O_5 \text{ or } V_2O_3 \text{ or VxOy} + xLi^+ + xe^- \quad (4)$$

Equations 1 and 2 represent the reduction reaction while eqs 3 and 4 represents the oxidation reactions. In its most favorable conditions we can expect that $InVO_4$ is able to react reversibly with 11 mol Li per mole, thus having a high theoretical capacity of 1283 mA h g^{-1}. We note above reactions are further verified by various spectroscopic studies like X-ray absorption, X-ray photoelectron spectroscopy (XPS), and infrared (IR) and Raman studies.

Electrochemical Impedance Spectroscopy. Electrochemical impedance spectroscopy (EIS) is one of the most informative analytical techniques that can be employed to understand reaction kinetics of the Li-ion insertion/deinsertion process in compounds due to its nondestructive nature and ability to differentiate various phenomena taking place in an electrode at different time periods.[14,27−29] Presently we studied the EIS studies on $InVO_4$ method II (900 °C), since it showed the most promising galvanostatic cycling result when compared to the other samples. EIS was carried out in the frequency range of 0.5 MHz to 3 mHz, with alternating current signal amplitude of 10 mV.

Figure 6b shows the Nyquist plot for the compound during various discharge voltages starting from the open circuit voltage (OCV, 2.8 V) of the cell. Figure 6a shows the Nyquist plot of a specific discharge voltage (0.005 V). The width of the semicircles was found to increase steadily with the decrease in the discharge voltage. Figure 6c shows the equivalent circuit used to fit the impedance spectra.

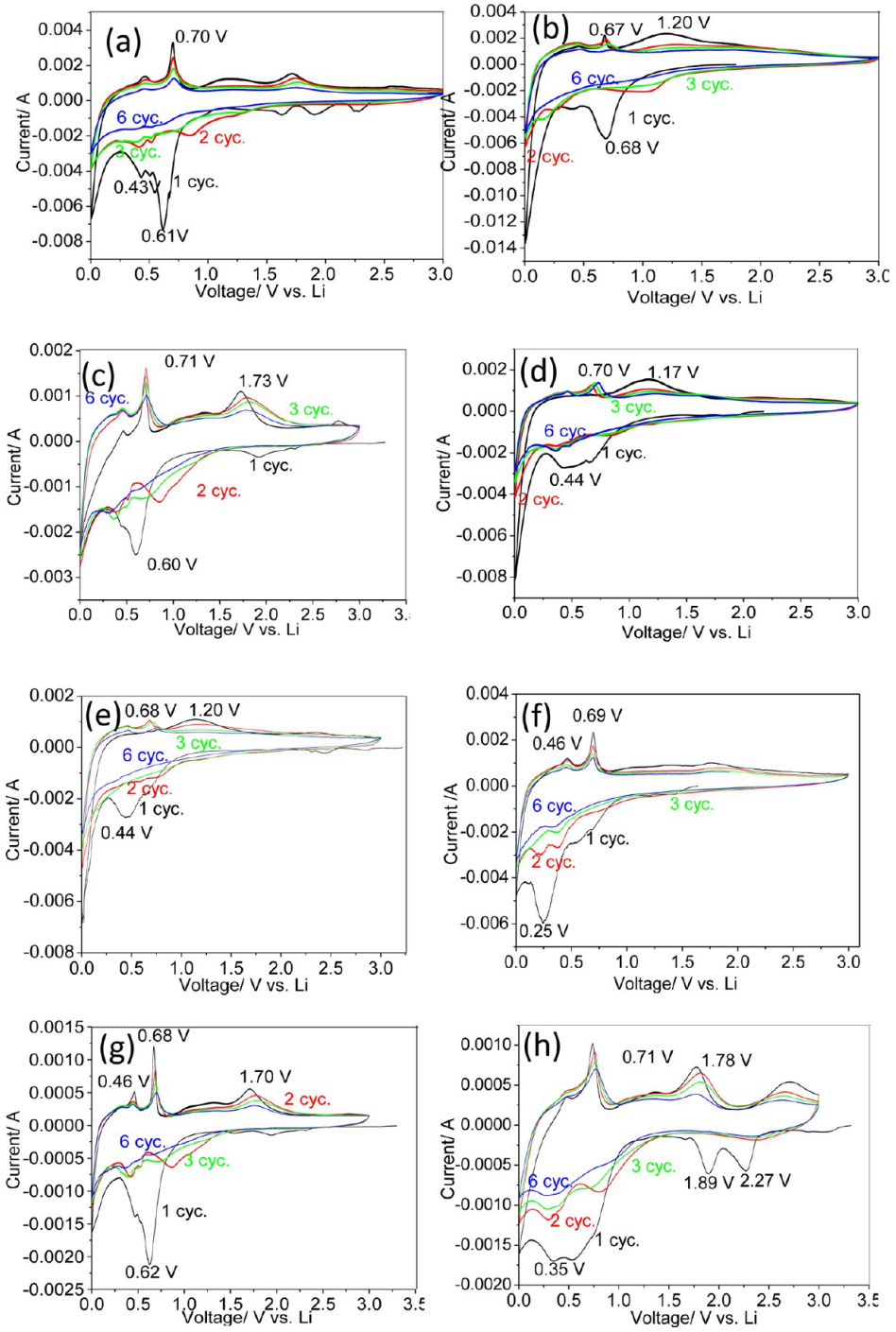

Figure 3. Cyclic voltammograms recorded at a scan rate of 58 mV s^{-1} in the range 0.005−3.0 V vs Li: (a) method I, (b) method II (bare-500 °C), (c) method II (reheated-900 °C), (d) method III (bare), (e) method III (EDTA), (f) method IV, (g) method V (bare), (h) method V (reheated-500 °C).

As seen in Figure 6a for the 0.005 V discharge voltage, the first semicircle observed at the high frequency region was due to the process of the surface film resistance (R_{sf}) and middle frequency region is due to charge transfer resistance (R_{ct}). Surface film resistance arises due to the migration of Li^+ ions through the solid electrolyte interface (SEI) film.[29] Charge transfer resistance, on the other hand, is the Li^+ ion charge-transfer resistance at the interface between the electrode and electrolyte.[29] The second semicircle observed at lower frequencies corresponds to the bulk phenomena, R_b, which is the electronic resistivity of the $InVO_4$ anode material and ionic conductivity of the $LiPF_6$ electrolyte in the pores of the composite electrode consisting of the following: active material, conducting Super-P carbon, and the binder due to inhomogeneous coating of active material onto the current collector. The semicircles would usually be followed by the appearance of straight line Warburg type region, W_s.

The impedance spectra were analyzed by fitting all the discharge and charge voltages to an equivalent electrical circuit slightly modified from the circuit by Nobili et al.[30] composed

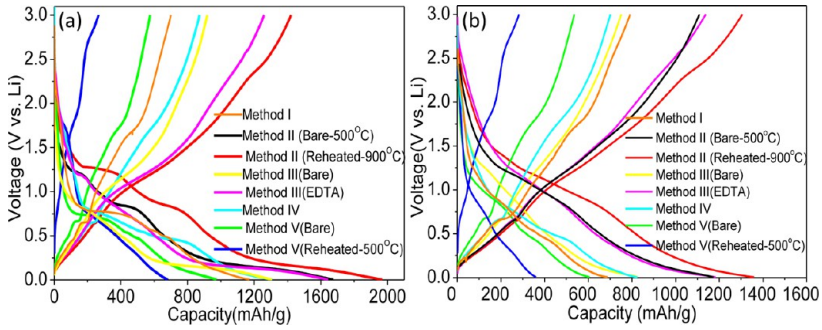

Figure 4. Galvanostatic cycling studies of (a) 1st and (b) 2nd cycle charge and discharge of $InVO_4$ prepared by the different preparation methods (I–V).

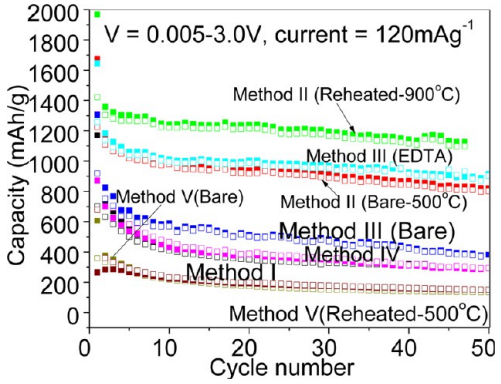

Figure 5. Capacity against cycle number graph of $InVO_4$ prepared by different methods: current rate 120 mA g^{-1}, voltage range 0.005–3.0 V vs Li.

Table 2. Reversible Capacity Values and Capacity Fading Values of $InVO_4$ Prepared by Different Methods

preparation method	reversible capacity at 1st cycle (±5; mAh g^{-1})	reversible capacity at 20th cycle (±5; mAh g^{-1})	capacity retention (%; 2nd to 50th cycles; cycling range)
I	1171	362	88 (2–40 cyc)
II (500 °C)	1421	940	78
II (900 °C)	1420	1241	87 (2–48 cyc)
III	918	523	68
III (EDTA)	1259	1002	85
IV	872	388	76
V	606	183	46
V (reheated)	679	199	57

of: R_e (combined resistance of electrolyte and cell components); R_{sf+ct} (resistance due to surface film and charge transfer); CPE_{sf+dl} (capacitance due to surface film and double layer); CPE_b (bulk capacitance); R_b (bulk resistance); W_s (Warburg impedance); C_{int} (intercalation capacitance). The circuit is shown in Figure 6c. Most of the times, only one semicircle would be seen in the high-to-medium-frequency range, as seen in Figure 6b where all the different discharge voltages are plotted, indicating that effects due to surface film resistance and charge transfer resistance are not separable. Therefore, instead of having two separate resistances (R_{sf} and R_{ct}) and their respective constant phase elements (CPE_{sf} and CPE_{ct}), a proper assignment would instead be R_{sf+ct} and CPE_{sf+dl}. CPE_b values are much higher, in the order of millifarads, as compared to CPE_{sf+dl}, which is in the order of microfarads, since it does not only include bulk impedance of

Table 3. Impedance Parameters of $InVO_4$ during Charge-Discharge Cycles at Various Voltages[a]

voltage/V vs Li	R_e/Ω	R_{sf+ct}/Ω	$CPE_{sf+dl}/\mu F$	R_b/Ω	CPE_b/mF	W_s/Ω
discharge cycle						
OCV	7.0	56.2	26.2			130
2.0	8.8	83.4	23.0			182
1.8	9.5	71.2	23.6			299.5
1.6	7.2	71.8	28.6			189.4
1.4	4.5	80.4	27.9			143.3
1.2	2.1	74.1	29.4			184.3
1.0	5.7	79.4	27.8	16.1	7.9	327.4
0.8	5.2	75.9	31.3	22.3	7.1	208.4
0.6	4.7	71.3	32.4	29.9	10.4	156.3
0.4	4.5	76.3	27.4	37.3	9.3	165.5
0.2	4.5	77.4	31.1	37.3	8.4	129.3
0.1	4.3	80.0	28.5	40.4	8.4	146.4
0.005	4.3	80.6	28.3	43.6	8.2	174.8
charge cycle						
0.1	4.0	81.7	32.0	28.0	13.7	143.8
0.2	3.9	82.1	32.3	27.2	13.9	103.6
0.4	4.1	74.2	28.6	27.7	12.4	137.3
0.6	4.0	77.5	31.0	26.1	12.2	170.7
0.8	3.3	44.6	22.3			425.9
1.0	3.7	36.5	44.1			301.5
1.2	3.8	32.9	44.1			244.2
1.4	4.5	36.1	5.311			299.2
1.6	4.9	32.8	41.7			382.1
1.8	4.8	36.5	58.7			791.7
2.0	5.6	25.7	17.6			630.1
2.2	5.7	26.7	19.0			634.6
2.4	5.6	31.1	22.9			662.2
2.6	5.5	35.1	31.4			715
2.8	4.2	39.3	145.5			716.6
3.0	3.9	29.2	152.8			919.3

[a]Error values: R_{sf+ct} = ±5 Ω, CPE_{sf+dl} = ±5 μF, R_b = ±3 Ω, CPE_b = ±3 mF, W_s = ±0.5 Ω.

the anode material but also that from the electrolyte trapped in the electrode pores. A constant phase element (CPE) was used in the equivalent circuit instead of pure capacitance due to the observation of depressed semicircle indicative of inhomogeneous surface. Further details on equivalent electrical circuit notations are discussed by Reddy et at.[29] W_s is the Warburg resistance associated with the solid state diffusion of Li-ion through the $InVO_4$ lattice. However, the R_b and CPE_b circuit element components were only included in the equivalent

dx.doi.org/10.1021/am401501a | ACS Appl. Mater. Interfaces 2013, 5, 7777–7785

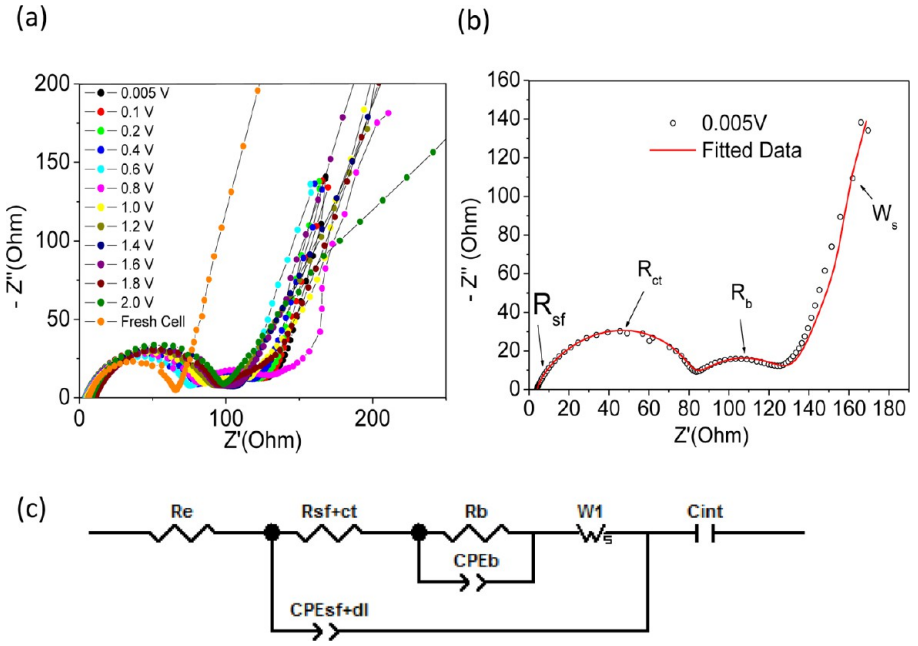

Figure 6. Electrochemical impedance spectroscopy (EIS) studies of method II (reheated-900 °C). Nyquist plots (Z′ vs −Z″) during (a) the discharge cycle, (b) select voltage (0.005 V) fitted with equivalent electrical circuit. The symbols are the experimental data, whereas the continuous line is the fitted data. (c) Equivalent electrical circuit used to fit the experimental impedance spectra.

circuit for voltages of the impedance spectra where the bulk phenomena was observed at lower frequencies.

The impedance data values are summarized in Table 3. Due to changes in the electrode kinetics, these impedance parameters will exhibit a variation as a function of voltage during charge−discharge cycling. The R_{sf+ct} and R_b values were found to increase with the discharge voltage during discharge cycle and decrease with the charge voltage during charge cycle. R_{sf+ct} was 56.2 Ω at OCV but steadily increased to 80.6 Ω at the end of the discharge cycle at 0.005 V. During charge cycle, it decreased from 81.72 to 29.2 Ω by the end of the charge cycle. Similarly, R_b increased from 16.1 to 43.6 Ω during discharge cycle and decreased from 28.0 to 26 Ω by the end of the charge cycle. EIS studies clearly showed impedance values are highly sensitive to voltages in charged or discharged state. However, bulk impedance resistance was only included in the electrical circuit from 1.0 V onward and from 0.6 V onward for discharge and charge cycles respectively when there was the appearance of the second semicircle corresponding to bulk impedance. Warburg resistance (W_s) values were reletively low. EIS studies shows that impedance values are dependent on the cell voltage.

CONCLUSIONS

$InVO_4$ was successfully synthesized using the five different preparation methods and under different preparation conditions. The compound was then characterized using XRD, scanning electron microscope (SEM), density measurements, and BET surface area methods, showing differing morphology throughout the different preparation methods and under the different conditions. In addition to main orthorhombic phase, a small amount of impurities (In_2O_3 and V_2O_5) were found. Electrochemical studies were done to determine the suitability of the compound created using different methods in being an alternative anode material. Galvanostatic cycling at 120 mA g^{-1} in voltage range, 0.005−3.0 V vs Li/Li^+ showed that method II (reheated-900 °C) gave the highest capacity of 1241 mA h g^{-1} after the 20th cycle, close to the theoretical capacity of 1283 mA h g^{-1}, equivalent to 11 mol of Li ion transferred per mole $InVO_4$ per cycle. In addition, its capacity was also relatively steady, with a capacity fading of only 13%. Reaction mechanisms were proposed based on alloy-dealloying reaction and conversion reactions using cyclic voltammograms and charge−discharge cycling. EIS studies was further investigated on method II (reheated-900 °C) to understand more about the reaction kinetics. In conclusion, five different preparation methods have been demonstrated for feasibility. The different preparation methods employed can produce widely different physical and electrochemical properties. This shows the importance of choosing the suitable preparation methods and conditions when synthesizing alternative anode materials. While some methods produced undesirable cycling profiles due to high capacity fading and relatively low capacity value, methods II and III showed good cycling results and can potentially be used as an for lithium-ion batteries. For further optimization of its anodic properties, other parameters, such as heat treatment of the prepared electrodes, reduce the In content by low cost elements, understanding mechanisms and attempts on reduction of discharge−charge voltages of $InVO_4$ anode material in the future.

ASSOCIATED CONTENT

Supporting Information

Galvanostatic cycling profiles of $InVO_4$ prepared by different methods I−V: (a) method I, (b and c) method II, (d and e) method III, (f) method IV, and (g and h) method V: current rate 120 mA g^{-1}; voltage range 0.005−3.0 V. This material is available free of charge via the Internet at http://pubs.acs.org.

AUTHOR INFORMATION

Corresponding Author

*E-mail: phymvvr@nus.edu.sg; msemvvr@nus.edu.sg; reddymvvr@gmail.com. Telephone number: +65-65162607. Fax: +65-67776126.

Notes

The authors declare no competing financial interest.

■ ACKNOWLEDGMENTS

M.V.R. thanks MOE-GEB & Faculty of Science for the grant WBS N-144-000-005-001 and the National Research Foundation (NRF) Singapore NRF-CRP for grant nos. R-144-000-295-281 and R-143-000-360-281.

■ REFERENCES

(1) Goodenough, J. B.; Kim, Y. *Chem. Mater.* **2010**, *22*, 587−603.
(2) Reddy, M. V.; Subba Rao, G. V.; Chowdari, B. V. R. *Chem. Rev.* **2013**, *113*, 5364−5457.
(3) Ellis, B. L.; Lee, K. T.; Nazar, L. F. *Chem. Mater.* **2010**, *22*, 691−714.
(4) Denis, S.; Baudrin, E.; Touboul, M.; Tarascon, J. M. *J. Electrochem. Soc.* **1997**, *144*, 4099−4109.
(5) Li, B. X.; Wang, Y. F. *Mater. Res. Bull.* **2010**, *45*, 1903−1908.
(6) Reddy, M. V.; Sakunthala, A.; Selvasekarapandian, S.; Chowdari, B. V. R. *J. Phys. Chem. C* **2013**, *117*, 9056−9064.
(7) Sakunthala, A.; Reddy, M. V.; Selvasekarapandian, S.; Chowdari, B. V. R.; Selvin, P. C. *Energy Environ. Sci.* **2011**, *4*, 1712−1725.
(8) Le Viet, A.; Reddy, M. V.; Jose, R.; Chowdari, B. V. R.; Ramakrishna, S. *J. Phys. Chem. C* **2010**, *114*, 664−671.
(9) Christe, T. C.; Reddy, M. V.; Sow, C. H.; Chowdari, B. V. R. *ACS Appl. Mater. Interfaces* **2013**, *5*, 918−923.
(10) Reddy, M. V.; Yu, C.; Jiahuan, F.; Loh, K. P.; Chowdari, B. V. R. *ACS Appl. Mater. Interfaces* **2013**, *5*, 4361−4366.
(11) Reddy, M. V.; Yu, T.; Sow, C. H.; Shen, Z. X.; Lim, C. T.; Subba Rao, G. V.; Chowdari, B. V. R. *Adv. Funct. Mater.* **2007**, *17*, 2792−2799.
(12) Sharma, Y.; Sharma, N.; Subba Rao, G. V.; Chowdari, B. V. R. *Adv. Funct. Mater.* **2007**, *17*, 2855−2861.
(13) Saravanan, K.; Balaya, P.; Reddy, M. V.; Chowdari, B. V. R.; Vittal, J. J. *Energy Environ. Sci.* **2010**, *3*, 457−464.
(14) Sakunthala, A.; Reddy, M. V.; Selvasekarapandian, S.; Chowdari, B. V. R.; Selvin, P. C. *J. Phys. Chem. C* **2010**, *114*, 8099−8107.
(15) Oh, S. W.; Park, S. H.; Sun, Y. K. *J. Power Sources* **2006**, *161*, 1314−1318.
(16) Reddy, M. V.; Subba Rao, G. V.; Chowdari, B. V. R. *Electrochim. Acta* **2005**, *50*, 3375−3382.
(17) Tey, S. L.; Reddy, M. V.; Subba Rao, G. V.; Chowdari, B. V. R.; Yi, J. B.; Ding, J.; Vittal, J. J. *Chem. Mater.* **2006**, *18*, 1587−1594.
(18) Reddy, M. V.; Pecquenard, B.; Vinatier, P.; Levasseur, A. *Electrochem. Commun.* **2007**, *9*, 409−415.
(19) Varghese, B.; Reddy, M. V.; Yanwu, Z.; Lit, C. S.; Hoong, T. C.; Subba Rao, G. V.; Chowdari, B. V. R.; Wee, A. T. S.; Lim, C. T.; Sow, C. H. *Chem. Mater.* **2008**, *20*, 3360−3367.
(20) Park, C. M.; Kim, J. H.; Kim, H.; Sohn, H. J. *Chem. Soc. Rev.* **2010**, *39*, 3115−3141.
(21) Murugan, A. V.; Reddy, M. V.; Campet, G.; Vijayamohanan, K. *J. Electroanal. Chem.* **2007**, *603*, 287−296.
(22) Leroux, F.; Goward, G. R.; Power, W. P.; Nazar, L. F. *Electrochem. Solid-State Lett.* **1998**, *1*, 255−258.
(23) Leroux, F.; Nazar, L. F. *Solid State Ionics* **2000**, *133*, 37−50.
(24) Reddy, M. V.; Subba Rao, G. V.; Chowdari, B. V. R. *J. Solid State Electrochem.* **2013**, *17*, 1765−1773.
(25) Reddy, M. V.; Kenrick, K. Y. H.; Wei, T. Y.; Chong, G. Y.; Leong, G. H.; Chowdari, B. V. R. *J. Electrochem. Soc.* **2011**, *158*, A1423−A1430.
(26) Reddy, M. V.; Yu, C.; Jiahuan, F.; Loh, K. P.; Chowdari, B. V. R. *RSC Adv.* **2012**, *2*, 9619−9625.
(27) Reddy, M. V.; Jose, R.; Teng, T. H.; Chowdari, B. V. R.; Ramakrishna, S. *Electrochim. Acta* **2010**, *55*, 3109−3117.
(28) Reddy, M. V.; Subba Rao, G. V.; Chowdari, B. V. R. *J. Mater. Chem.* **2011**, *21*, 10003−10011.
(29) Reddy, M. V.; Subba Rao, G. V.; Chowdari, B. V. R. *J. Phys. Chem. C* **2007**, *111*, 11712−11720.
(30) Nobili, F.; Dsoke, S.; Croce, F.; Marassi, R. *Electrochim. Acta* **2005**, *50*, 2307−2313.